JOURNAL OF GEOPHYSICAL RESEARCH, VOL. 108, NO. B11, 2545, doi:10.1029/2001JB000474, 2003

Stress drops and radiated energies of aftershocks of the 1994 Northridge, California, earthquake

Jim Mori
Disaster Prevention Research Institute, Kyoto University, Uji, Kyoto, Japan

Rachel E. Abercrombie
Department of Earth and Planetary Sciences, Boston University, Boston, Massachusetts, USA

Hiroo Kanamori
Seismological Laboratory, California Institute of Technology, Pasadena, California, USA

Received 1 December 2000; revised 11 May 2003; accepted 25 June 2003; published 28 November 2003.

[1] We study stress levels and radiated energy to infer the rupture characteristics and scaling relationships of aftershocks and other southern California earthquakes. We use empirical Green functions to obtain source time functions for 47 of the larger ($M \geq 4.0$) aftershocks of the 1994 Northridge, California earthquake (M6.7). We estimate static and dynamic stress drops from the source time functions and compare them to well-calibrated estimates of the radiated energy. Our measurements of radiated energy are relatively lowcompared to the static stress drops, indicating that the static and dynamic stress drops are of similar magnitude. This is confirmed by our direct estimates of the dynamic stress drops. Combining our results for the Northridge aftershocks with data from other southern California earthquakes appears to show an increase in the ratio of radiated energy to moment, with increasing moment. There is no corresponding increase in the static stress drop. This systematic change in earthquake scaling from smaller to larger (M3 to M7) earthquakes suggests differences in rupture properties that may be attributed to differences of dynamic friction or stress levels on the faults. *INDEX TERMS:* 7215 Seismology: Earthquake parameters; 7209 Seismology: Earthquake dynamics and mechanics; 7230 Seismology: Seismicity and seismotectonics; 8164 Tectonophysics: Stresses—crust and lithosphere; *KEYWORDS:* Northridge, aftershocks, stress energy, California, source parameters

Citation: Mori, J., R. E. Abercrombie, and H. Kanamori, Stress drops and radiated energies of aftershocks of the 1994 Northridge, California, earthquake, *J. Geophys. Res.*, *108*(B11), 2545, doi:10.1029/2001JB000474, 2003.

1. Introduction

[2] We investigate the relationship between stress drops (static and dynamic) and radiated energy using well-determined source parameters for a set of Northridge aftershocks and other southern California earthquakes. The 1994 Northridge earthquake (M_w6.7) was a large damaging event in southern California [*U.S. Geological Survey*, 1996], and the well-recorded main shock and aftershock sequence have been the focus of numerous seismological and engineering studies [e.g., *Consortium of Universities for Research in Earthquake Engineering*, 1998]. Estimates of the radiated energy and stress drop provide information about the mechanics of earthquake ruptures and help distinguish between models that describe the tectonic and frictional stress levels before, during, and after the earthquake (e.g., models described in the work of *Lachenbruch and Sass* [1980] and *Kikuchi and Fukao* [1988]). Although earthquake stress drops reflect only the relative changes in stress, we can use our results to make inferences about the absolute levels of tectonic stress. *Lachenbruch and Sass* [1980] used radiated seismic energies to infer low stress levels (<20 MPa) on the San Andreas fault. In a similar way, we determine estimates of the radiated energy and use them to infer the tectonic stress level for the southern California region. We discuss our observations of radiated energy and stress drop in the context of simple models that describe the stress and friction conditions during the earthquake.

[3] We also investigate how source parameters vary as a function of earthquake size. Recent observations have suggested that as earthquakes increase in magnitude they radiate an increasingly larger proportion of energy [*Kanamori et al.*, 1993; *Abercrombie*, 1995; *Mayeda and Walter*, 1996], which implies differences from standard constant stress drop models [e.g., *Aki*, 1967; *Kanamori and Anderson*, 1975]. Small (M_L − 1 to 5) earthquakes recorded at Cajon Pass borehole show a relative increase of radiated energy with magnitude, without a corresponding increase in static stress drop [*Abercrombie and Leary*, 1993; *Abercrombie*, 1995]. This study looks at larger magnitude (M4−5) events to investigate if the same trend exists. Systematic changes in

0148-0227/03/2001JB000474$09.00

the relative amounts of energy radiated as a function of event size could indicate important differences in the rupture dynamics of small and large earthquakes [*Kanamori and Heaton*, 2000].

[4] Using well-resolved source time functions derived from empirical Green function deconvolutions, we obtain reliable estimates of stress drops and radiated energy. We then investigate the relationships between these source parameters to provide constraints on the stresses driving the earthquakes and source scaling for $M4$ to $M7$ earthquakes.

2. Data and Method

[5] Earthquake source parameter studies are always complicated by difficulties in separating source and propagation effects in the waveforms. This problem is somewhat simplified for larger earthquakes ($M > 4$) recorded at distances of less than 50 km since there are usually clear body wave arrivals and wave propagation effects, such as attenuation and multiple arrivals, that are less dominant at the relevant frequencies. Large aftershock sequences that are recorded with modern instrumentation provide the opportunity to study a significant number of such earthquakes. This was the case following the 1994 Northridge earthquake ($M6.7$) when an active aftershock sequence with numerous large events was recorded by high-quality permanent and portable stations in southern California.

[6] We examined all the aftershocks with magnitude greater or equal to M_L 4.0 from January 1994 to May 1995 and selected the earthquakes that had clean P wave arrivals for which we can obtain clear Green function deconvolutions. We discarded earthquakes mainly whose P wave arrival is contaminated by other events. This occurred largely on the first day following the main shock when aftershocks were occurring at a high rate. This exclusion left 47 of the large ($M \geq 4.0$) Northridge aftershocks (Table 1) for our estimates of source parameters. These earthquakes were recorded on broadband Terrascope [*Kanamori*, 1991] stations and the temporary station LA00 operated by University of California, Santa Barbara (Figure 1). We use hypocenters determined with a three-dimensional velocity model, which improves the depth determinations [*Mori et al.*, 1995]. Focal mechanisms and seismic moments were determined by *Thio and Kanamori* [1996] using regional surface waves. All data in this study are obtained from the southern California Earthquake Center Data Center.

3. Empirical Green Functions

[7] We use empirical Green function deconvolutions to remove path and site effects from the P waveforms [e.g., *Mueller*, 1985; *Mori and Frankel*, 1990] and extract source time functions. The waveform of a small earthquake is used as an empirical Green function to remove the path and site effects from the waveform of a larger target earthquake. This results in a waveform corresponding to the far-field source time function of the target earthquake. One of the important aspects of this method is choosing an appropriate small earthquake for use as the empirical Green function. We examine a large number of small earthquakes to find a good empirical Green function and try deconvolutions using all small events within an epicentral radius of 2 km and with magnitudes larger than $M1.5$ and at least 1.5 units smaller than the target earthquake. We do not limit the depth range because of possible uncertainties in the depth determinations for these small earthquakes. Within the Northridge aftershock zone, this search pattern usually yielded several tens to several hundreds of potential empirical Green function events.

[8] Figure 2 shows a typical range of waveforms that are obtained for the deconvolutions using 37 different, small earthquakes. This subset of 37 events includes all the $M2.0$ and greater earthquakes located in 1994 within an epicentral radius of 2.0 km and with depths within 2.0 km of target earthquake (CUSP ID 3143547). The deconvolved waveforms are ordered by increasing interevent epicentral distance between the Green function and target earthquakes. It is difficult to estimate accurately the resolution of the relative locations, but it is thought to be on the order of several hundred meters. For the smaller interevent spacings, the results are better but there are some deconvolutions at closer distances that do not work well and some deconvolutions at greater distances that produce good waveforms. The variation in the quality of the resultant source time functions in Figure 2 shows only a weak dependence on the interevent distance and suggests caution in using waveform similarities to infer relative locations of earthquakes. In addition to the close distances, similar focal mechanisms (which are usually unavailable for these small events) are probably important factors for choosing an appropriate empirical Green function. The choice of the Green function that is used in this study is a subjective judgment made by looking at the deconvolved waveforms. One positive aspect of this technique is that the empirical Green functions that result in clear deconvolved waveforms all give generally consistent results. The waveforms in Figure 2 that have good signal-to-noise ratios (traces plotted with darker lines) show fairly similar shapes with comparable source durations. The event chosen for the deconvolution has an interevent spacing of 1.2 km.

[9] All the source time functions used in this study are shown in Figure 3. The amplitudes of the waveforms are adjusted so that the areas of the displacement pulse are proportional to the long-period moments. This normalization allows direct comparison of the amplitudes of the source time functions. The derived source time functions are ordered by size so that waveforms with similar amplitudes are plotted together.

4. Source Parameters

4.1. Source Radius

[10] Using the source time functions obtained from the empirical Green function deconvolutions, we estimate the pulse durations as shown in Figure 3 and summarized in Table 2. As a simple classification of pulse shapes, we also qualitatively identify each source time function as either a "simple" or "complex" waveform.

[11] *Deichmann* [1999] discussed the problem of estimating pulse durations because of the ambiguity of picking the onset in the deconvolution. We can largely avoid this problem because the onsets are generally clear in the

Table 1. Northridge Aftershocks Analyzed in This Study

Year	Mo	Da	Time	Latitude	Longitude	Mag.	Depth	ID
94	1	17	12 39 39.79	34.265	−118.540	4.9	13.2	3144652
94	1	17	12 54 33.74	34.307	−118.459	4.0	2.0	2150608
94	1	17	12 55 46.83	34.277	−118.578	4.1	6.0	3140674
94	1	17	13 6 28.34	34.251	−118.550	4.6	0.1	3140678
94	1	17	13 26 45.00	34.318	−118.456	4.7	6.0	3140684
94	1	17	13 56 2.48	34.293	−118.621	4.4	2.0	3140691
94	1	17	14 14 30.63	34.332	−118.445	4.5	2.8	3140870
94	1	17	15 7 3.17	34.304	−118.474	4.2	1.6	3140728
94	1	17	15 7 35.46	34.307	−118.467	4.1	1.0	2138698
94	1	17	15 54 10.76	34.376	−118.627	4.8	12.7	3140766
94	1	17	17 56 8.21	34.228	−118.573	4.6	19.2	3140853
94	1	17	19 35 34.30	34.311	−118.456	4.0	1.2	3140898
94	1	17	19 43 53.38	34.368	−118.637	4.1	11.4	3141205
94	1	17	20 46 2.40	34.302	−118.565	4.9	6.4	3141219
94	1	17	22 31 53.73	34.339	−118.442	4.1	0.1	3141242
94	1	17	23 33 30.69	34.326	−118.698	5.6	4.9	3141273
94	1	17	23 49 25.36	34.342	−118.665	4.0	8.2	3141062
94	1	18	0 43 8.89	34.376	−118.698	5.2	8.4	3141286
94	1	18	4 1 26.72	34.358	−118.623	4.3	0.5	3141180
94	1	18	7 23 56.02	34.333	−118.623	4.0	12.7	3141341
94	1	18	15 23 46.89	34.379	−118.561	4.8	7.1	3141597
94	1	19	4 40 48.00	34.361	−118.571	4.3	1.6	3142081
94	1	19	9 13 10.90	34.304	−118.737	4.1	13.0	3142087
94	1	19	14 9 14.83	34.215	−118.510	4.5	18.2	3142198
94	1	19	21 9 28.61	34.379	−118.712	5.1	14.4	3142595
94	1	19	21 11 44.90	34.378	−118.619	5.1	9.7	3142597
94	1	21	18 39 15.26	34.301	−118.466	4.5	9.7	3145627
94	1	21	18 39 47.08	34.297	−118.479	4.0	8.6	3159009
94	1	21	18 42 28.77	34.310	−118.475	4.2	8.8	3143541
94	1	21	18 52 44.23	34.302	−118.452	4.3	9.0	3143546
94	1	21	18 53 44.57	34.298	−118.459	4.3	8.8	3143547
94	1	23	8 55 8.66	34.300	−118.427	4.1	8.1	3144303
94	1	24	4 15 18.82	34.347	−118.551	4.6	7.1	3145150
94	1	24	5 50 24.34	34.361	−118.628	4.3	9.4	3145168
94	1	24	5 54 21.07	34.364	−118.627	4.2	9.1	3145171
94	1	27	17 19 58.83	34.273	−118.563	4.6	13.4	3146628
94	1	28	20 9 53.43	34.375	−118.494	4.2	2.1	3146983
94	1	29	11 20 35.97	34.306	−118.579	5.1	1.1	3147406
94	1	29	12 16 56.35	34.278	−118.611	4.3	2.7	3147259
94	2	3	16 23 35.37	34.300	−118.440	4.0	8.8	3149105
94	2	6	13 19 27.02	34.292	−118.476	4.1	9.0	3150210
94	2	25	12 59 12.59	34.357	−118.480	4.0	2.3	3155150
94	3	20	21 20 12.26	34.231	−118.475	5.2	12.5	3159411
94	5	25	12 56 57.05	34.312	−118.393	4.4	8.5	3169078
94	6	15	5 59 48.63	34.311	−118.398	4.1	8.9	3172383
94	12	6	3 48 34.49	34.293	−118.389	4.5	9.5	3195727
95	6	26	8 40 28.94	34.394	−118.669	5.0	13.3	3217586

original data. Knowing the time of the onsets in the original data, we can calculate the start time of the deconvolved pulse. The onsets of the source time functions are not picked from the pulse of the deconvolved waveforms but instead are calculated from the onsets of the original data.

[12] Converting the pulse duration into an estimate of the source dimension (r) presents some uncertainty since any method is model dependent and also depends on the take-off angle (θ) from the fault plane, which is not always known. We use the relationship of *Boatwright* [1980], which assumes a circular rupture model,

$$r = \tau_{1/2} v/(1 - v/\alpha \sin\theta), \quad (1)$$

where $\tau_{1/2}$ is the risetime (assumed to be 0.5 times the total duration), α is the depth-dependent P wave velocity (Table 3), and v is the rupture velocity assumed to be 0.75β. An average value for $\sin\theta$ of 0.64 is assumed for the takeoff angle.

[13] Even for source time functions that seem to have simple shapes, there are still ambiguities in picking the source duration. For example, in event 3142198, we pick a rather short duration ($\sim$0.1 s) of the source time function (upper right on second portion of Figure 3), which results in a small source area and rather high static stress drop. However, for the same event, Boatwright (personal communication) uses spectral empirical Green functions to pick corner frequencies and obtains a rather low corner frequency (2.4 Hz), which gives a significantly larger source area and thus gives a much lower (factor of 5) stress drop. These uncertainties and differences in interpretation of the waveforms demonstrate some of the problems in trying to estimate source areas of small earthquakes.

4.2. Static Stress Drop

[14] The static stress drop is the difference between the final and starting stress levels on the fault, and it is measured by determining the ratio of the slip to the fault

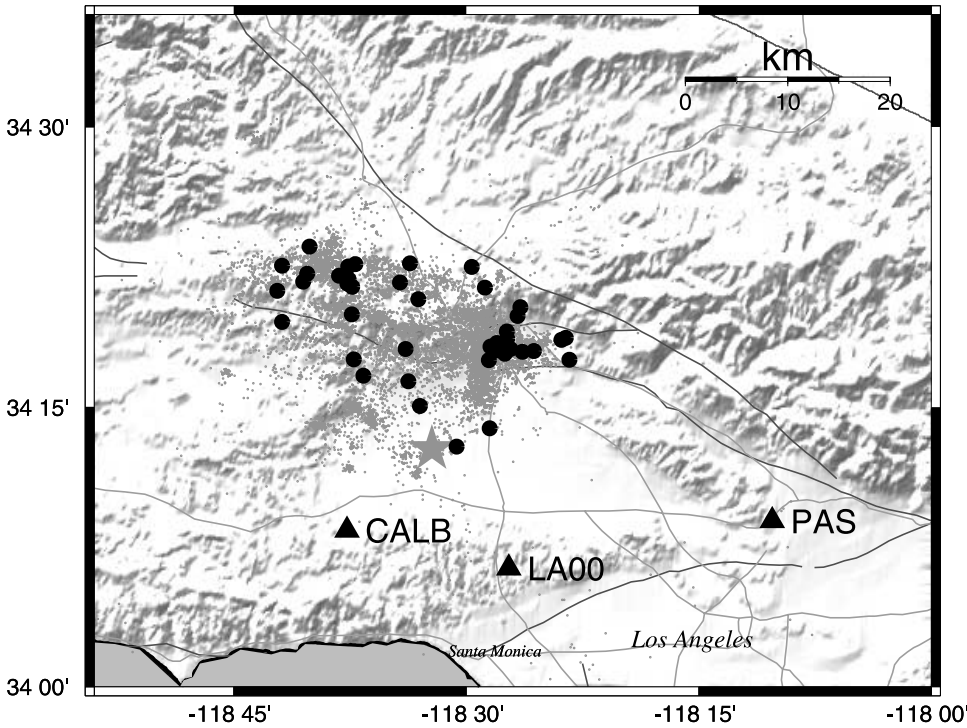

Figure 1. Map showing locations of Northridge aftershocks (solid circles) and stations (solid triangles) used in this study. Shaded star and small dots show locations of Northridge main shock and distribution of smaller aftershocks, respectively.

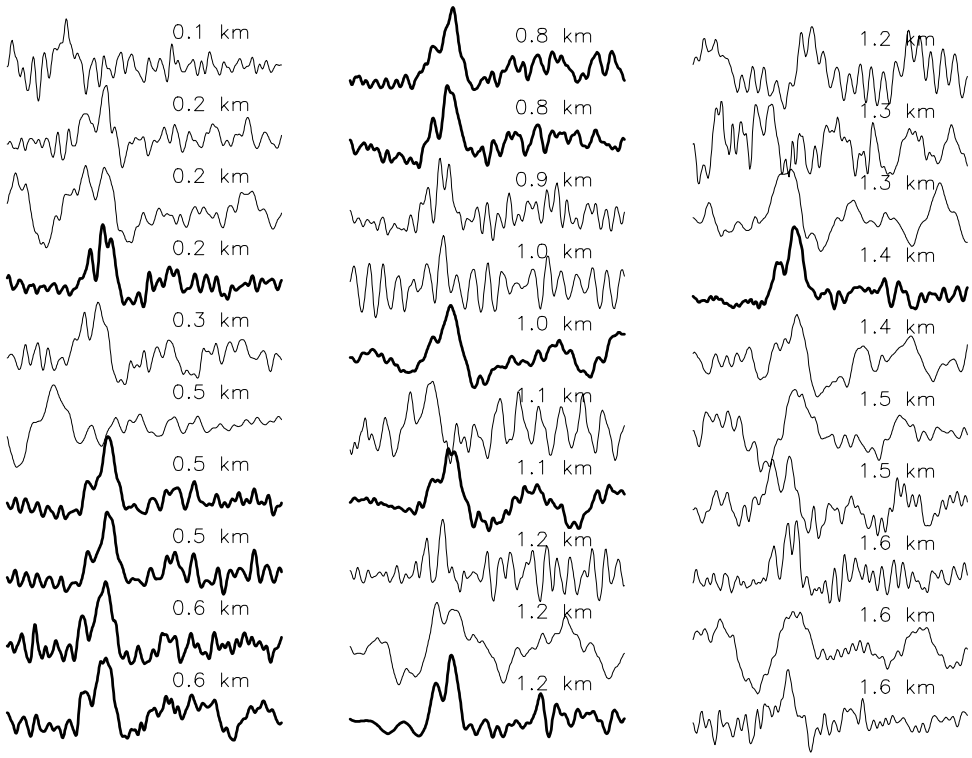

Figure 2. Deconvolutions for a subset of the small events that were tested as empirical Green functions for event 3143547 recorded at LA00. The number above each time series shows the interevent distance. The traces plotted with heavier lines show deconvolutions with better signal-to-noise ratio. The bottom seismogram in the middle column was used for the source parameter estimate.

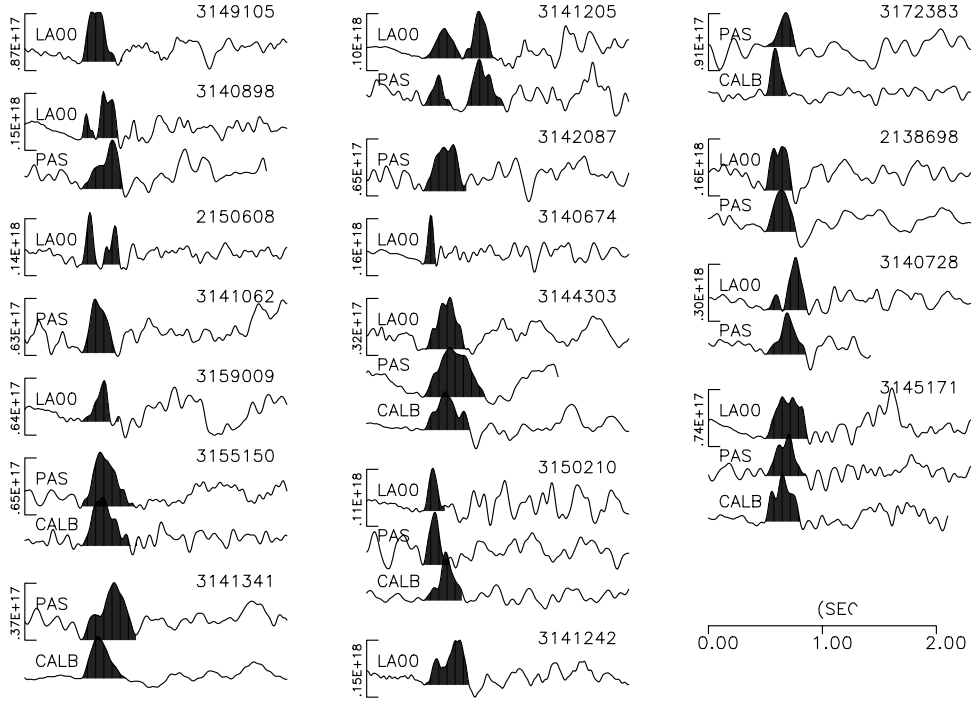

Figure 3. Source time functions of Northridge aftershocks used in this study derived from deconvolution of empirical Green functions. Shaded portions show duration used for estimates of source dimension and static stress drop. Vertical scale (Nm/s) shows the amplitude such that the area of the shaded portions equal the seismic moments.

dimension. In this study, the static stress drop ($\Delta\sigma_s$) is calculated using the formula of *Eshelby* [1957],

$$\Delta\sigma_s = (7/16)M_o/r^3, \quad (2)$$

where M_o is the seismic moment. There is a difference in interpreting the static stress drops for simple and complex earthquakes, which can be seen if we compare two earthquakes that have equal moments and total durations. If one earthquake ruptured in a single event, while the other had several subevents, the actual static drops could be significantly different. For example, if the second earthquake was made up of two equal-sized circular subevents, its static stress drop would be a factor of 4 higher than the single event. A

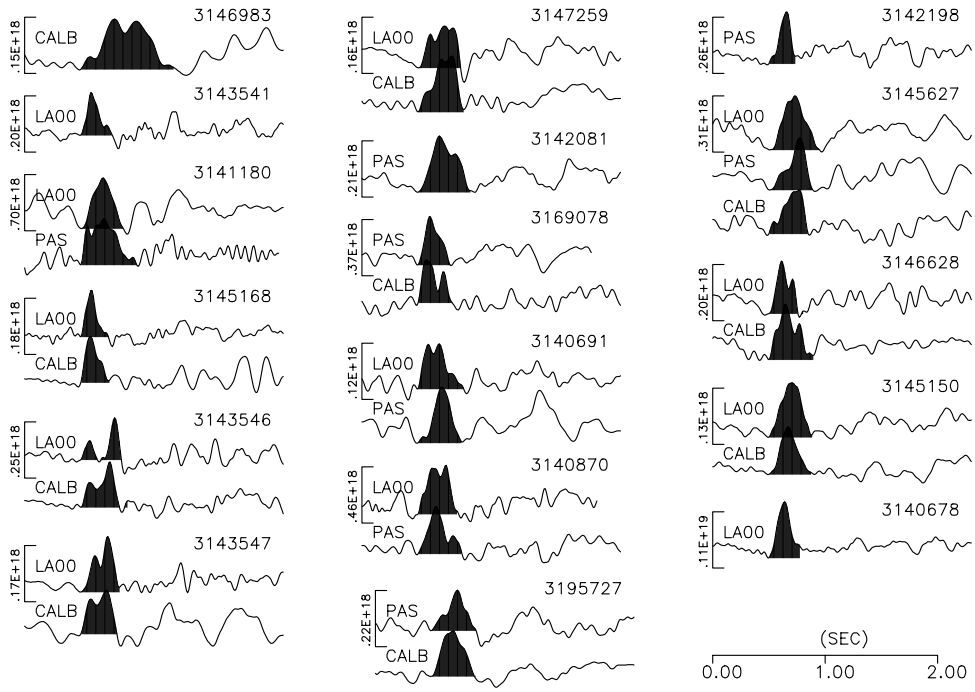

Figure 3. (continued)

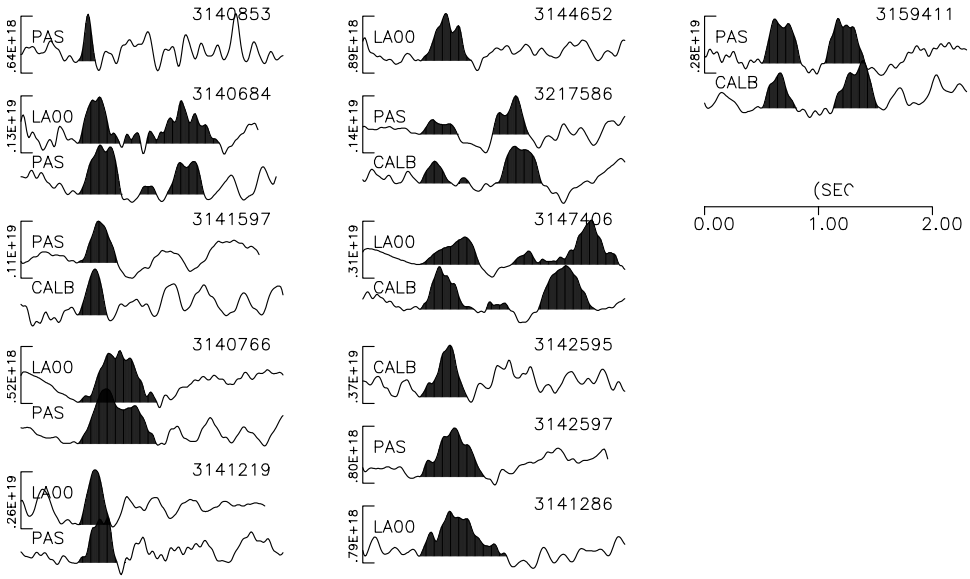

Figure 3. (continued)

good example of a complex earthquake is event 3159411, which has two clear subevents of about the same size. We calculate the static stress drops for all the earthquakes using the total duration of the source pulse. For complex earthquakes that have distinguishable subevents, we also estimate the static stress drop for the first subevent.

4.3. Dynamic Stress Drop

[15] The dynamic stress drop is defined as the tectonic driving stress minus the dynamic frictional stress and is proportional to the slip velocity of the fault [*Dahlen*, 1974]. We follow the work of *Kanamori and Heaton* [2000] and define the "average" dynamic stress drop ($\langle\Delta\sigma_d\rangle$) as the initial stress (σ_0) minus the average frictional stress ($\langle\sigma_d\rangle$):($\langle\sigma_d\rangle$) = $\sigma_0 - \langle\sigma_f\rangle$. The "initial" dynamic stress drop ($\Delta\sigma_d$) is simply the initial stress (σ_0) minus the frictional stress early in the rupture (σ_f): $\Delta\sigma_d = \sigma_0 - \sigma_f$. If the frictional stress is constant during rupture, then the two dynamic stress drops are the same ($\Delta\sigma_d = \langle\Delta\sigma_d\rangle$), as shown in Figure 4a.

[16] Assuming a self-similar crack growth at the beginning of a rupture, *Boatwright* [1980] derived a formula for determining the dynamic stress drop ($\Delta\sigma_d$) from the initial slope of the far-field velocity pulse. We estimate $\Delta\sigma_d$ from the deconvolved source time functions (Figure 3) after differentiating once. We measure the initial slope ($\dot{u}/t$) for the first 0.05–0.1 s, which corresponds to 15–30% of the duration. We then estimate $\Delta\sigma_d$ using the expression below derived by combining Boatwright's equations (5) and (40).

$$\Delta\sigma_d = M_O(4\pi)^{-1}\left(1-\zeta^2\right)^2 v^{-3}\bar{u}^{-1}\dot{u}/t, \tag{3}$$

where $(1 - \varsigma^2)^2$ is a geometrical factor, which was assumed to have the average value of 0.75, and $\bar{u}$ is the area of the source time function. Since the initial slope of the waveform is measured, this estimate of dynamic stress drop is for the beginning part of the rupture. If the dynamic properties, such as friction, change with time, then the value of dynamic stress drop will also change, and $\Delta\sigma_d \neq \langle\Delta\sigma_d\rangle$.

[17] *Kanamori and Heaton* [2000] obtained the following relation between radiated energy (E_s), static stress drop ($\Delta\sigma_s$) and $\langle\Delta\sigma_d\rangle$:

$$2\mu E_S/M_O = (2\langle\Delta\sigma_d\rangle - \Delta\sigma_S). \tag{4}$$

where μ is the rigidity. We thus use our measurements of energy, moment, and static stress drop to calculate the average dynamic stress drops. We use a depth-dependent rigidity, determined from the shear wave velocity (Table 3).

4.4. Apparent Stress

[18] The apparent stress, σ_e, was introduced by *Wyss and Brune* [1968]

$$\sigma_e = \mu E_S/M_O. \tag{5}$$

In this study, we calculate the apparent stress using the radiated energy and the depth-dependent rigidity. Although it is difficult to interpret the apparent stress as a physical stress level, the apparent stress is a measure of the ratio of the radiated energy to the moment. Replacing the moment by fault slip (D) and fault area (A), the apparent stress can be written as

$$\sigma_e = (E_S/A)/D. \tag{6}$$

In this expression, the apparent stress can be interpreted as the seismic energy radiated, per unit fault area, per unit fault slip.

4.5. Radiated Energy

[19] We estimate radiated energy (E_s) from the integral of the squared velocity records ($\int V^2 dt$) for the duration of the seismograms on three components, following the work of *Kanamori et al.* [1993]:

$$E_S = 2.36\times 10^7 R^2[R_O q\ (R_O)\ ]^2/\ [Rq(R)]^{-2}\int V^2\,dt, \tag{7}$$

where E_s is in Joules with hypocentral distance R in meter and V in meter per second. The distance-attenuation

Table 2. Source Parameters Determined for Northridge Aftershocks[a]

ID	Moment, Nm	Dur., s	E_S, J	Static Stress, MPa	App. Stress, MPa	Dyn. Stress, MPa	Simple/Complex
3144652	2.20E + 16	0.48		0.9	13.3	3.78	s
2150608	1.00E + 15	0.38	6.40E + 10 0.53	2.9	0.72	8.66	c
	5.50E + 14	0.20	10.9				
3140674	1.00E + 15	0.11	0.00E + 00 0.19	65.2		5.69	s
3140678	7.90E + 15	0.33	1.70E + 11 0.46	34.8	0.24	34.65	s
3140684	1.10E + 16	1.21	2.40E + 11 2.08	0.5	0.36	4.43	c
	5.30E + 15	0.36	10.2				
3140691	4.00E + 15	0.42	1.20E + 11 0.59	8.6	0.34		c
3140870	5.60E + 15	0.39	9.00E + 10 0.55	14.4	0.18		s
3140728	2.00E + 15	0.38	2.30E + 10 0.53	6.0	0.12	4.12	c
	2.40E + 14	0.09	44.3				
2138698	1.40E + 15	0.30	3.20E + 10 0.41	8.6	0.26	8.81	s
3140766	1.60E + 16	0.71	5.20E + 11 1.33	3.0	0.62	1.89	s
3140853	7.00E + 15	0.18	0.38	57.6		12.25	s
3140898	1.00E + 15	0.36	8.50E + 09 0.51	3.4	0.10	5.28	c
3141205	2.50E + 15	0.71	1.20E + 10 1.32	0.5	0.10	0.43	c
	9.70E + 14	0.30	2.5				
3141219	3.50E + 16	0.36	9.90E + 11 0.62	65.1	0.46	25.3	s
3141242	1.40E + 15	0.41	1.20E + 10 0.58	3.2	0.10	5.20	c
3141062	1.00E + 15	0.29	0.50	3.6		1.22	s
3141286	4.00E + 16	0.77	1.32	7.6			s
3141180	6.00E + 15	0.44	6.90E + 10 0.62	10.8	0.12	20.36	s
3141341	1.00E + 15	0.45	2.20E + 10 0.85	0.7	0.42	0.28	s
3141597	1.70E + 16	0.34	4.40E + 11 0.58	37.5	0.42	17.4	s
3142081	2.60E + 15	0.47	4.60E + 10 0.66	4.0	0.20	3.46	s
3142087	1.40E + 15	0.37	0.69	1.8			s
3142198	4.80E + 15	0.23	1.90E + 11 0.48	18.9	0.94	1.4	s
3142595	8.50E + 16	0.46	0.86	58.4	2.92		s
3142597	2.50E + 16	0.68	2.20E + 12 1.17	6.9	1.42	5.69	s
3145627	7.50E + 15	0.41	1.80E + 11 0.70	9.7	0.38	1.74	s
3159009	7.50E + 15	0.33	0.57	18.1	0.70	0.91	
3143541	2.00E + 15	0.34	0.58	4.4	7.28	0.22	s
3143546	2.40E + 15	0.42	2.60E + 10 0.72	2.8	0.18	2.37	c
	7.90E + 14	0.09	111.9				
3143547	2.40E + 15	0.41	6.60E + 10 0.71	2.9	0.44	1.03	c
3144303	5.40E + 14	0.48	1.20E + 10 0.82	0.4	0.36	0.42	s
3145150	2.50E + 15	0.38	1.00E + 11 0.66	3.8	0.64	1.58	s
3145168	2.20E + 15	0.25	4.30E + 10 0.43	12.2	0.32	3.56	s
3145171	1.70E + 15	0.39	2.20E + 10 0.67	2.5	0.20	0.94	s
3146628	3.20E + 15	0.35	1.10E + 11 0.65	5.0	0.66	1.10	c
3146983	3.50E + 15	0.82	1.60E + 10 1.15	1.0	0.06		s
3147406	6.30E + 16	1.74	2.44	1.9		20.79	c
	2.30E + 16	0.49	32.4				
3147259	1.70E + 15	0.39	2.20E + 10 0.55	4.4	0.14	2.31	s
3149105	1.40E + 15	0.35	1.80E + 10 0.60	2.8	0.20	2.06	s
	2.10E + 14	0.15	9.9				
3150210	7.70E + 14	0.25	2.00E + 10 0.42	4.5	0.42	1.82	s
3155150	7.30E + 14	0.48	6.70E + 09 0.67	1.1	0.10	1.27	s
3159411	1.20E + 17	1.02	4.20E + 12 1.91	7.6	0.68	28.63	c
	5.30E + 16	0.30	130.7				
3169078	4.60E + 15	0.31	7.60E + 10 0.54	12.8	0.26	8.7	c
3172383	8.70E + 14	0.26	2.30E + 10 0.45	4.3	0.42	1.40	s
3195727	3.40E + 15	0.50	2.00E + 11 0.85	2.4	0.96	1.74	s
3217586	4.10E + 16	1.09	1.20E + 12 2.12	18.7	0.56	2.92	c
	1.10E + 16	0.30		74.0			

[a]Entries without ID numbers are source parameter estimates for the first subevent of the event listed above. "s" and "c" stand for simple and complex events, respectively.

relationship $q(R) = 2.27 \times 10^3 R^{-1.22} \exp(-5.3R)$, and R_o = 8 km is the radius of the sphere used for the energy estimated. We use broadband velocity records at distances of 10–100 km. Typically, 5–10 stations are used for each earthquake providing good azimuthal coverage and giving a fairly stable estimate. An important part of this process that improves the reliability of the radiated energy determination is the use of empirical station corrections. These empirical corrections for the individual station amplitudes considerably reduce the scatter of estimates for a particular event [*Kanamori et al.*, 1993].

Table 3. One-Dimensional Velocity Model Derived From *Mori et al.* [1995]

Depth, km	P Velocity, km/s	S Velocity, km/s
0	4.5	2.6
5	5.5	3.2
10	6.0	3.5
16	6.7	3.9

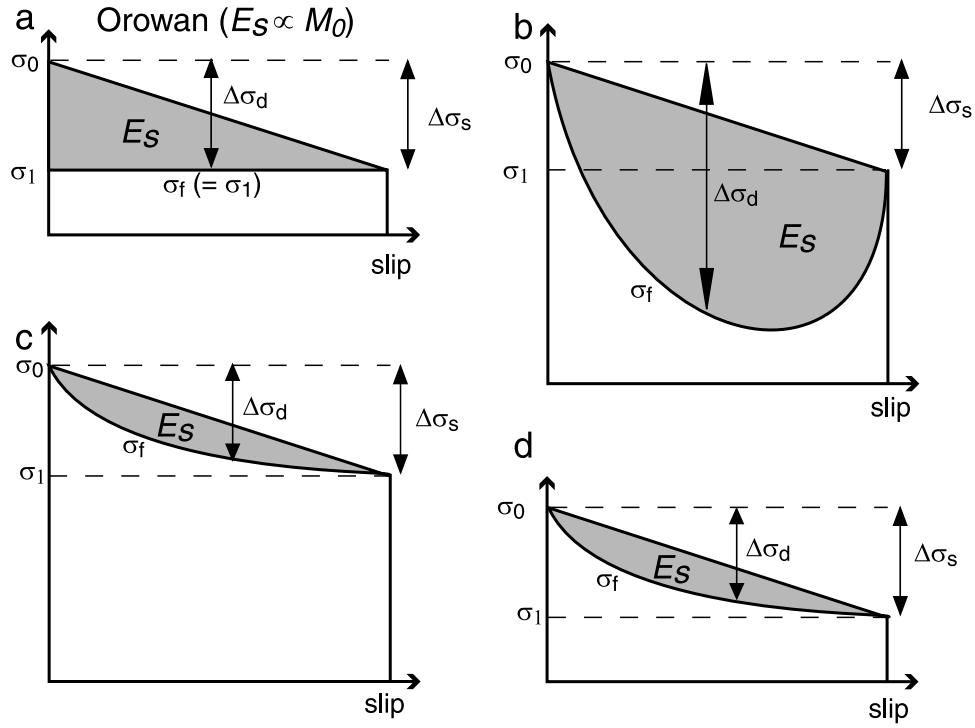

Figure 4. Range of schematic models illustrating the relationship between stress levels for an earthquake. (a) The Orowan model. (b) Model with a varying frictional stress that drops below the final stress. (c and d) Models with varying frictional stress that do not drop below the final stress. The difference between Figures 4c and 4d is the different average stress levels. The measurements of energy in this study are lower than the Orowan case, so the suggested model Figures 4c and 4d may be appropriate.

4.6. Relation Between Stress Drops and Energy

[20] The relation between the various types of stress drops can be confusing, especially when considering faults with strongly heterogeneous stress release. In a simple fault model (Figure 4a), if the dynamic frictional stress is constant throughout the earthquake rupture (assuming uniform driving stress), the initial dynamic stress drop is equal to the average dynamic stress drop and to the static stress drop. This is the classic *Orowan* [1960] model of stress release of an earthquake (although other models can also give these simple relationships). The dynamic stress drop we calculate in this study from the initial portion of the waveform is closer to the initial dynamic stress drop than the average dynamic stress drop. In this simple model, the radiated energy is directly proportional to the moment, and so the apparent stress is constant for all size earthquakes, assuming constant static stress drop. The apparent stress is thus half of the average dynamic stress drop.

[21] Summarizing the above statements for the Orowan model,

$$\Delta\sigma_d = \Delta\sigma_s = \langle\Delta\sigma_d\rangle = 2\sigma_e. \tag{8}$$

[22] The physical mechanisms for fault slip in an earthquake are certainly more complicated than the simple Orowan model. For understanding the rupture process, the levels of frictional stress on the fault during the earthquake are especially important. Comparing these various estimates of stress drop in this study allows us to investigate the

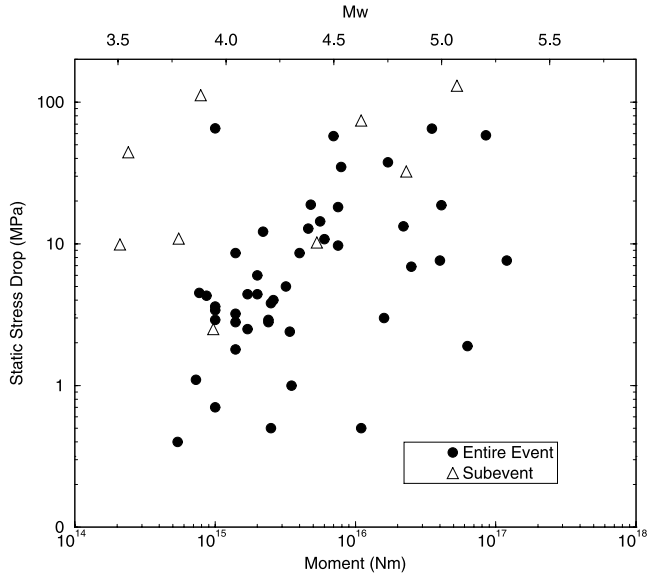

Figure 5. Static stress drops plotted as a function of moment for larger Northridge aftershocks (solid circles). The open triangles are estimates of static stress drops and moments of clear subevents from complex source time functions.

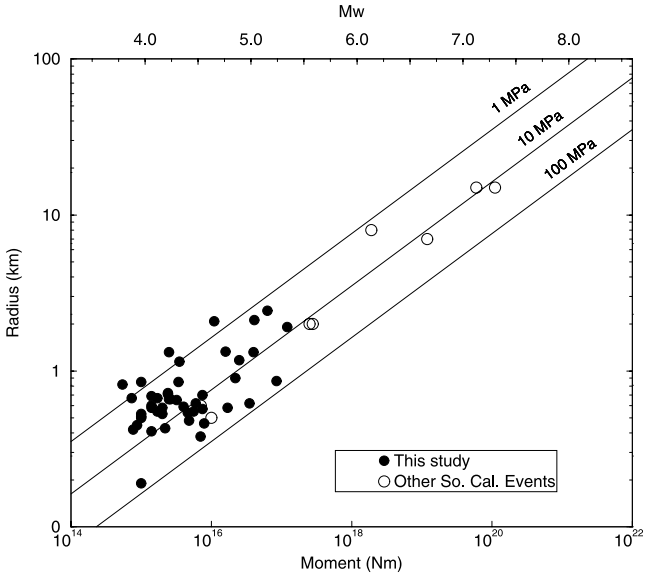

Figure 6. Source radius plotted as a function of moment for larger Northridge aftershocks (solid circles) and several other large southern California earthquakes (open circles).

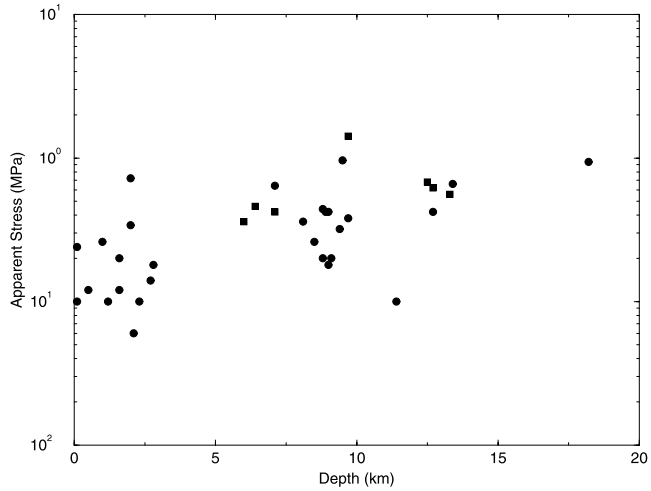

Figure 8. Apparent stress plotted as a function of source depth for larger Northridge aftershocks. The data are divided into two size groups (less than and greater than 10^{16} Nm) since there is a moment dependence of the radiated energy.

scaling of radiated energy as a function of earthquake size and to make some inferences about the stress levels for these earthquakes in southern California.

5. Results

[23] The source parameters we obtain for the larger Northridge aftershocks are listed in Table 2 and shown in Figures 5–9. There is a large range in the static stress drops from a few tens to several tens of mega pascals, but the values do not seem to show a strong correlation with earthquake size (Figure 5) or event depth. For the "entire event" data in Figure 5, there seems to be a trend of increasing static stress drop with moment, but it is hard to evaluate such trends over this limited moment range. In order to extend the earthquake moment range, Figure 6 shows the estimates of source radius as a function of moment, including data from other studies of larger southern California earthquakes that had reliable estimates of moment and fault size (Table 4). Similar to the results of *Kanamori and Anderson* [1975] and *Abercrombie and Leary* [1993], Figure 6 indicates that there is no systematic increase in static stress drop as a function of earthquake size.

[24] When we combine our data from Northridge aftershocks with other data from recent southern California earthquakes (Table 4), Figure 7 shows that the ratio of E_s/M_o

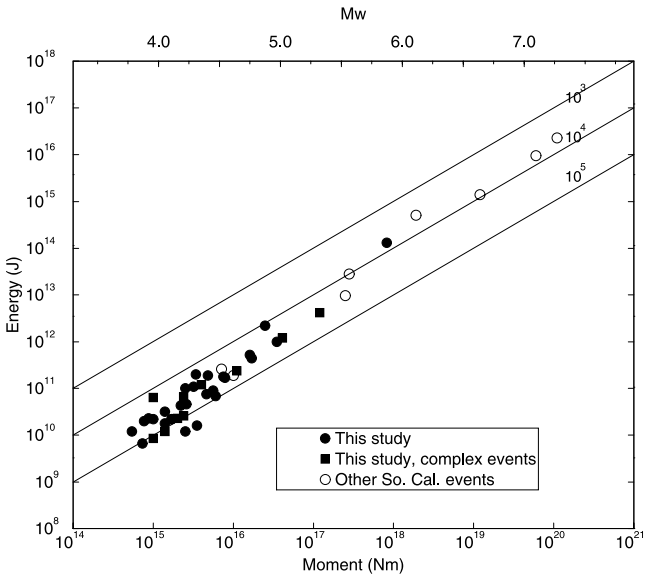

Figure 7. Radiated energy plotted as a function of moment for larger Northridge aftershocks analyzed in this study. Circles and squares represent simple and complex events, respectively. Data from other studies of southern California earthquakes are also shown (open circles).

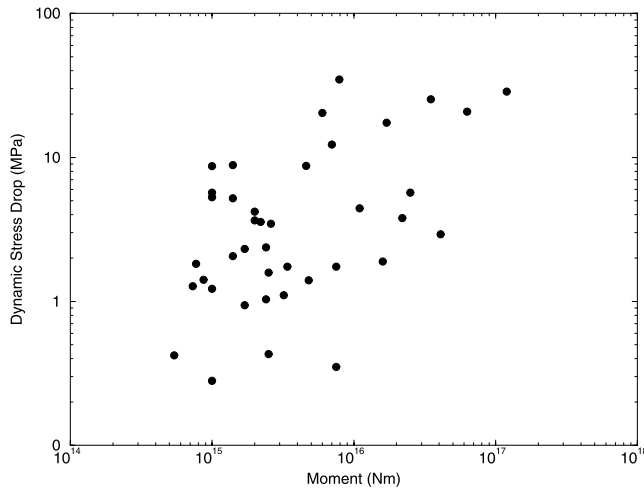

Figure 9. Plot of dynamic stress drop, calculated from the slope of the velocity pulse, as a function of seismic moment.

Table 4. Source Parameters for Southern California Earthquakes Determined in Other Studies

	Moment, Nm	Energy, J	Radius, km
Upland (1,2) 2/28/90	2.5×10^{17}	9.7×10^{12}	2
Sierra Madre (2,3) 6/28/91	2.8×10^{17}	2.8×10^{13}	2
Landers (4,5) 6/28/92	1.1×10^{20}	8.6×10^{15}	15[a]
Northridge (5,6,7) 1/17/94	1.2×10^{19}	1.4×10^{15}	7
Northridge Aftershocks (6,8) 1/17/94 1733	8.2×10^{17}	2.0×10^{13}	
4/26/97	1.0×10^{16}	1.9×10^{11}	0.5
4/27/97	7.1×10^{15}	2.6×10^{11}	0.6
Hector Mine (4,5,9) 10/16/99	6.0×10^{19}	3.4×10^{15}	15[a]

[a]For long strike-slip faults, this value is the fault width. (1), *Dreger*, 1993; (2), *Kanamori et al.*, 1993; (3), *Wald*, 1992, 1995; (4), *Venkataraman*, 2002; (5), Harvard moment tensor catalog, *Dziewonski et al.*, 1981; (6), J. Boatwright, personal communication, 2001; (7), *Wald et al.*, 1996; (8), *Venkatarama et al.*, 2000; (9), *Boatwright et al.*, 2002.

gradually increases as a function of earthquake moment. For the smaller events (10^{15}–10^{16} Nm) the ratio of energy to moment is 10^{-5} to 10^{-6}, while for the larger events ($>10^{16}$ Nm) the ratio increases to between 10^{-5} and 10^{-4}. This study shows that there appears to be a slight relative increase in the amount of radiated energy, as a function of earthquake moment, without a corresponding increase in the static stress drop. This observation is similar to the results for smaller earthquakes from the work of *Abercrombie* [1995]. Overall, the values of radiated energy are relatively small and indicate that the static and dynamic stress drops are roughly equivalent, if the model assumptions of equation (4) are correct.

[25] It is unlikely that the relatively small amounts of energy radiated by the earthquakes in this study (Figure 7) can be explained by attenuation effects. The values are about a factor of 10 smaller than for the larger earthquakes, which means a factor of $\sqrt{10}$ in actual amplitudes since the measurements are made from velocity-squared data. It seems unlikely that we are systematically underestimating the radiated energy of the smaller events by greater than a factor of 3 in the frequency range of 1–5 Hz. This is the frequency range that has been traditionally used for determining local magnitudes in southern California, so the distance attenuation has been extensively studied [e.g., *Jennings and Kanamori*, 1983; *Hutton and Boore*, 1987].

[26] Figure 7 also distinguishes between the simple and complex earthquakes in the Northridge aftershocks. One possible explanation for the larger ratio of radiated energy to moment for the larger earthquakes is that the larger events tend to be more complex. Thus the large earthquakes have relatively more high-frequency content and generate more radiated energy. From our simple classification of source complexity, we see no indication of this.

[27] Figure 8 shows the apparent stress (σ_e) as a function of earthquake depth. Since we show above that there is a dependence of radiation on earthquake size, when we look for depth dependence, we divided the data into two subsets with events of moments less than and greater than 10^{16} Nm. In Figure 8 there appears to be a trend of increasing apparent stress with earthquake depth, indicating that the deeper earthquakes are radiating relatively more energy than the shallow ones. One might obtain this apparent trend if the larger aftershocks systematically occurred at greater depth. This is not the case with our data set, which has a fairly even depth distribution for the range of aftershocks.

[28] Figure 9 shows the dynamic stress drop, as calculated from the initial slope of the velocity waveform, plotted as a function of seismic moment. There appears to be a trend of increasing dynamic stress drop with earthquake size. However, similar to Figure 5, with the large amount of scatter in the data, it is difficult to evaluate such trends over limited moment ranges.

6. Discussion

[29] Our study shows that there is a large range of static stress drops for the Northridge aftershocks (0.5–60 MPa). Some of this scatter may be due to problems in correctly estimating the source duration because of uncertainties such as deconvolution errors and rupture directivity. Since we are using only one to three stations for each event, there is a limited azimuthal distribution, and we have not taken into account rupture directivity, which can significantly affect the observed source duration [e.g., *Mori*, 1996; *Venkataraman et al.*, 2000]. Despite these large uncertainties, we do not think that they can account for the range of static stress drops that spans nearly two orders of magnitude.

[30] The range of apparent stress is generally an order of magnitude smaller than our estimates of the dynamic ($\Delta\sigma_d$) and static ($\Delta\sigma_s$) stress drops. This implies that ($2\Delta\sigma_d - \Delta\sigma_s$) is a relatively small number, and the static and dynamic stress drops have values of the same order of magnitude. This is consistent with our independently calculated values of the dynamic and static stress drops, which have roughly similar values. One potential problem in our results is that there is no correlation between the estimated values of apparent stress and dynamic stress drop (correlation coefficient 0.09), which may indicate some large uncertainties with our estimates of apparent stress.

[31] Figure 4 shows several simple models of earthquake stress release that we use for interpreting our results. We show the models as stress-displacement ($\sigma_f - \Delta u$) diagrams as has been used by *Lachenbruch and Sass* [1980] and *Kikuchi and Fukao* [1988]. For an earthquake rupture, these diagrams show the stress levels on the vertical axis as a function of the fault displacement (slip times of the surface area). The shaded region shows the amount of radiated energy. Model A is the classical *Orowan* [1960] model which shows a static stress drop from the initial stress to a final stress that is equal to the frictional stress. This model predicts constant scaling of earthquake moment with radiated energy for a constant stress drop. As mentioned above,

some recent observations indicate that this scaling does not hold over the large range of earthquake sizes. Also, from equation (6), the absolute amount of observed radiated energy is not as large as that predicted by this model.

[32] Models B and C show two possibilities with varying dynamic frictional stress that can account for different amounts of radiated energy. Model B has a large drop of dynamic friction and generates large amounts of radiated energy with a large dynamic stress drop, while model C has much smaller radiated energy and smaller dynamic stress drop. The relatively low observations of E_s/M_o in this study and the comparable estimates of dynamic and static stress drop suggest that model C is preferable to model B. If model B correctly described earthquake ruptures, the ratio of E_s/M_o (which is proportional to twice the average dynamic stress drop minus the static stress drop from equation (4)) should be more than an order of magnitude larger than what is observed, and there should be much larger dynamic stress drops. From studies of source time functions of large earthquakes, *Kikuchi and Fukao* [1988] and *Kikuchi* [1992] also favor a model similar to model C.

[33] For models B, C, and D, the final level of stress (σ_l) does not necessarily have to be at the same level as the frictional stress (σ_f). If the final level is higher than the frictional level, it is termed the ''locking'' case; if the levels are the same, it is termed the ''null'' case; and if the frictional stress is higher than the final stress, it is termed the ''overshoot'' case [*Lachenbruch and Sass*, 1980]. For the models in Figure 4, all show the ''null'' case.

[34] All the seismological observations of stress in earthquakes are stress drops and do not tell us about the absolute level of stress. It is difficult therefore to distinguish between models C and D which are the same except that the initial stress is 100 MPa for model C and 10 MPa for model D. Model estimates of the heat generation during earthquakes suggest that it is difficult to sustain values of sliding friction that are over 10 MPa if the fault zone is less than a few centimeters in width [*Kanamori and Heaton*, 2000]. If the sliding friction has such high values, large amounts of heat would be generated that may melt the fault [*Sibson*, 1973] or increase the fluid pressures that would reduce the effective normal stress [*Sibson*, 1973; *Lachenbruch*, 1980]. Either mechanism would significantly reduce the dynamic friction. These model-dependent arguments suggest that dynamic frictional stress in large earthquakes is low, indicating that the lower absolute stress levels of model D are more reasonable than the high stress levels of model C.

[35] If the dynamic friction is low and the dynamic stress drop is comparable in size to the static stress drop, then earthquakes would have nearly complete stress drops, and the initial tectonic stress has values roughly equivalent to the static stress drops. This would argue for the ''low stress'' interpretation of faults where stress-driving earthquakes are in the range of a few mega pascals to a few tens of mega pascals (tens to hundreds of bars) and not in the 100 MPa (kilobar) range. This is consistent with the idea that the San Andreas fault is a generally ''low-strength'' structure, [e.g., *Brune*, 1970; *Lachenbruch and Sass*, 1980; *Zoback et al.*, 1987] rather than ''high-strength'' [e.g., *McGarr and Gay*, 1978; *Hickman*, 1991]. On the other hand, data from borehole in situ stress measurements [e.g., *McGarr and Gay*, 1978] and laboratory experiments [e.g., *Byerlee*, 1978] indicate that friction levels are much higher, and crustal faults are driven by ''high stress.'' Occasional earthquakes do occur with very high stress drops, such as a few of the events in this study (e.g., 3140674, 3140853) and other earthquakes like the *M*4.9 Pasadena earthquake, which have stress drops in the 100-MPa range [*Kanamori et al.*, 1990]. This indicates that locally there can be higher levels of stress.

[36] Another result of this study is that there appears to be a relative increase of radiated energy as a function of earthquake size, without a corresponding increase in the static stress drop, as suggested by *Abercrombie* [1995] and *Kanamori and Heaton* [2000]. There is still uncertainty about this observation, and the conclusions depend greatly on the data sets that are included. *Ide and Beroza* [2001] showed that if the results of recording-band limitations and attenuation are taken into account then the apparent stress may not increase with moment. The dynamic stress drops also may be higher for the large earthquakes (Figure 9). The increase of E_s/M_o and higher average dynamic stress drop for larger earthquakes suggest that there may be a gradual change in the rupture process as a function of earthquake size. One explanation is that all earthquakes have the same level of dynamic frictional stress and the same static stress drop, but larger earthquakes have higher initial stress. An alternative explanation is that the average frictional stress is lower for larger earthquakes, for example, if it decreases with increasing slip.

[37] In contrast to our observations, which show that larger earthquakes radiate relatively more energy than smaller ones, *McGarr* [1999] proposed a constant upper bound to the apparent stress over a large range of earthquake magnitudes. McGarr argues for a constant maximum seismic efficiency for all events from laboratory scales to large earthquakes. The principal difference between the two approaches is probably that we are interpreting the average values of a parameter, while McGarr considered the maximum.

7. Conclusions

[38] 1. For the large aftershocks of the 1994 Northridge earthquake, there is a large range of static stress drops from a few tens to several tens of mega pascals. The values do not correlate strongly with earthquake size, especially when combined with other data for larger events in southern California.

[39] 2. We observe a relative increase of radiated energy as a function of earthquake size. The ratio of E_S/M_o is around 10^{-5} for smaller (10^{15} Nm) earthquakes and around 10^{-4} for larger ($>10^{16}$ Nm) earthquakes. This is not due to an increase in static stress drop and may be related to frictional properties on the fault. The effect of heat generation and consequent melting of the fault or fluid pressurization could cause larger earthquakes to radiate more energy.

[40] 3. There is a relative increase of apparent stress as a function of source depth, which may indicate that deeper earthquakes at higher normal stress experience lower dynamic friction and more complete stress drops.

[41] **Acknowledgments.** Data used in this study were provided by the SCEC Data Center. J. M. acknowledges support from the USGS during this study. We appreciated many helpful comments from John Boatwright, Art McGarr, and Allan Rubin, which significantly improved the paper.

References

Abercrombie, R., and P. Leary, Source parameters of small earthquakes recorded at 2.5 km depth, Cajon Pass, southern California: Implications for earthquake scaling, *Geophys. Res. Lett.*, *20*, 1511–1514, 1993.

Abercrombie, R. E., Earthquake source scaling relationships from −1 to 5 M_L using seismograms recorded at 2.5-km depth, *J. Geophys. Res.*, *100*, 24,015–24,036, 1995.

Aki, K., Scaling law of seismic spectrum, *J. Geophys. Res.*, *72*, 729–740, 1967.

Boatwright, J., A spectral theory for circular seismic sources, simple estimates of source dimension, dynamic stress drop, and radiated seismic energy, *Bull. Seismol. Soc. Am.*, *70*, 1–28, 1980.

Boatwright, J., G. L. Choy-George, and L. C. Seekins, Regional estimates of radiated seismic energy, *Bull. Seismol. Soc. Am.*, *92*, 1241–1255, 2002.

Brune, J. N., Tectonic stress and the spectra of seismic shear waves from earthquakes, *J. Geophys. Res.*, *75*, 4997–5009, 1970.

Byerlee, J. D., Friction of rocks, *Pure Appl. Geophys.*, *116*, 615–626, 1978.

Consortium of Universities for Research in Earthquake Engineering, *Proceedings of the NEHRP Conference and Workshop on Research on the Northridge, California Earthquake of January 17, 1994*, vol. 1, *Overview and Workshop Proceedings*, 134 pp., Curee Publ., Richmond, Calif., 1998.

Dahlen, F. A., On the ratio of *P*-wave to *S*-wave corner frequencies for shallow earthquake sources, *Bull. Seismol. Soc. Am.*, *64*, 1159–1180, 1974.

Deichmann, N., Empirical Green's functions: Comparison between pulse width measurements and deconvolution by spectral division, *Bull. Seismol. Soc. Am.*, *89*, 178–189, 1999.

Dreger, D., Modeling earthquakes with local and regional broadband data, Ph.D. thesis, Calif. Inst. of Technol., Pasadena, Calif., 1993.

Dziewonski, A. M., T.-A. Chou, and J. H. Woodhouse, Determination of earthquake source parameters from waveform data for studies of global and regional seismicity, *J. Geophys. Res.*, *86*, 2825–2852, 1981.

Eshelby, J. D., The determination of the elastic field of an ellipsiodal inclusion and related problems, *Proc. R. Soc. London, Ser. A*, *241*, 376–396, 1957.

Hickman, S., Stress in the lithosphere and the strength of active faults, *Rev. Geophys.*, *29*, 759–775, 1991.

Hutton, L. K., and D. M. Boore, The M_L scale in southern California, *Bull. Seismol. Soc. Am.*, *77*, 2074–2094, 1987.

Ide, S., and G. C. Beroza, Does apparent stress vary with earthquake size?, *Geophys. Res. Lett.*, *28*, 3349–3352, 2001.

Jennings, P., and H. Kanamori, Effect of distance on local magnitudes found from strong-motion records, including records from the 1979 Imperial Valley, California, earthquake, *Bull. Seismol. Soc. Am.*, *73*, 265–280, 1983.

Kanamori, H., TERRAscope and CUBE Project at Caltech, *EOS Trans. AGU*, *72*, 564–565, 1991.

Kanamori, H., and D. L. Anderson, Theoretical basis of some empirical relations in seismology, *Bull. Seismol. Soc. Am.*, *65*, 1023–1095, 1975.

Kanamori, H., and T. H. Heaton, Microscopic and macroscopic physics of earthquakes, in *Geocomplexity and the Physics of Earthquakes*, *Geophys. Monogr. Ser.*, vol. 120, edited by J. Rundle, D. L. Turcotte, and W. Klein, 147–161, AGU, Washington, D. C., 2000.

Kanamori, H., J. Mori, and T. H. Heaton, The 3 December 1988, Pasadena earthquake (M_L = 4.9) recorded with the very broadband system in Pasadena, *Bull. Seismol. Soc. Am.*, *80*, 483–487, 1990.

Kanamori, H., J. Mori, E. Hauksson, T. H. Heaton, L. K. Hutton, and L. M. Jones, Determination of earthquake energy release and M_L using terrascope, *Bull. Seismol. Soc. Am.*, *83*, 330–346, 1993.

Kikuchi, M., Strain drop and apparent strain for large earthquakes, *Tectonophysics*, *211*, 107–113, 1992.

Kikuchi, M., and Y. Fukao, Seismic wave energy inferred from long-period body waves inversion, *Bull. Seismol. Soc. Am.*, *78*, 1707–1724, 1988.

Lachenbruch, A. H., Frictional heating, fluid pressure, and the resistance to fault motion, *J. Geophys. Res.*, *85*, 6097–6112, 1980.

Lachenbruch, A. H., and J. H. Sass, Heat flow and energetics of the San Andreas fault zone, *J. Geophys. Res.*, *85*, 6185–6222, 1980.

Mayeda, K., and W. R. Walter, Moment, energy, stress drop, and source spectra of western United States earthquakes from regional coda envelopes, *J. Geophys. Res.*, *101*, 11,195–11,208, 1996.

McGarr, A., On relating apparent stress to the stress causing earthquake fault slip, *J. Geophys. Res.*, *104*, 3003–3012, 1999.

McGarr, A., and N. C. Gay, State of stress in the earth's crust, *Annu. Rev. Earth Planet. Sci.*, *6*, 405–436, 1978.

Mori, J., Rupture directivity and slip distribution of the *M*4.3 foreshock to the 1992 Joshua Tree earthquake, southern California, *Bull. Seismol. Soc. Am.*, *86*, 805–810, 1996.

Mori, J., and A. Frankel, Source parameters for small events associated with the 1986 North Palm Springs, California, earthquake determined using empirical Green Functions, *Bull. Seismol. Soc. Am.*, *80*, 278–295, 1990.

Mori, J., D. J. Wald, and R. L. Wesson, Overlapping faults planes of the 1971 San Fernando and 1994 Northridge, California earthquakes, *Geophys. Res. Lett.*, *22*, 1033–1036, 1995.

Mueller, C. S., Source pulse enhancement by deconvolution of an empirical Green's function, *Geophys. Res. Lett.*, *22*, 33–36, 1985.

Orowan, E., Mechanism of seismic faulting, *Geol. Soc. Am. Memo.*, *79*, 323–345, 1960.

Sibson, R. H., Interactions between temperature and pore-fluid pressure during earthquake faulting, a mechanism for partial or total stress relief, *Nature Phys. Sci.*, *243*, 66–68, 1973.

Thio, H. K., and H. Kanamori, Source complexity of the 1994 Northridge earthquake and its relation to aftershock mechanisms, *Bull. Seismol. Soc. Am.*, *86*, S84–S92, 1996.

U.S. Geological Survey, Northridge '94: A damaging urban earthquake, *U.S. Geol. Surv. Open File Rep.*, 96–263, 1996.

Venkataraman, A., Investigating the mechanics of earthquakes using macroscopic seismic parameters, Ph.D. dissertation, 169 pp., Calif. Inst. of Technol., Pasadena, Calif., 2002.

Venkataraman, A., J. Mori, H. Kanamori, and L. Zhu, Fine structure of the rupture zone of the April 26 and 27, 1997, Northridge aftershocks, *J. Geophys. Res.*, *105*, 19,085–19,093, 2000.

Wald, D., Strong motion and broadband teleseismic analysis of the 1991 Sierra Madre, California, earthquake, *J. Geophys. Res.*, *97*, 11,033–11,046, 1992.

Wald, D., T. H. Heaton, and K. W. Hudnut, The slip history of the 1994 Northridge, Californian earthquake determined from strong-motion, teleseismic, GPS, and leveling data, *Bull. Seismol. Soc. Am.*, *86*, 549–570, 1996.

Wyss, M., and J. N. Brune, Seismic moment, stress, and source dimensions for earthquakes in the California-Nevada region, *J. Geophys. Res.*, *73*, 4681–4694, 1968.

Zoback, M. D., et al., New evidence on the state of stress of the San Andreas fault system, *Science*, *238*, 1105–1111, 1987.

R. E. Abercrombie, Department of Earth and Planetary Sciences, Boston University, Boston, MA 02215, USA.

H. Kanamori, Seismological Laboratory, California Institute of Technology, Pasadena, CA 91125, USA.

J. Mori, Disaster Prevention Research Institute, Kyoto University, Gokasho, Uji, Kyoto 611-0011, Japan. (mori@rcep.dpri.kyoto-u.ac.jp)